Equivalent flaw time-of-flight diffraction sizing with ultrasonic phased arrays

Brady J. Engle, Lester W. Schmerr Jr, and Alexander Sedov

Citation: AIP Conf. Proc. **1511**, 895 (2013); doi: 10.1063/1.4789139
View online: http://dx.doi.org/10.1063/1.4789139
View Table of Contents: http://proceedings.aip.org/dbt/dbt.jsp?KEY=APCPCS&Volume=1511&Issue=1
Published by the American Institute of Physics.

EQUIVALENT FLAW TIME-OF-FLIGHT DIFFRACTION SIZING WITH ULTRASONIC PHASED ARRAYS

Brady J. Engle[1,2], Lester W. Schmerr Jr[1,2], and Alexander Sedov[3]

[1]Center for Nondestructive Evaluation, Iowa State University, Ames, IA 50011
[2]Department of Aerospace Engineering, Iowa State University, Ames, IA 50011
[3]Department of Mechanical Engineering, Lakehead University, Thunder Bay, ON, Canada

ABSTRACT. Ultrasonic phased array transducers can be used to extend traditional time-of-flight diffraction (TOFD) crack sizing, resulting in more quantitative information about the crack being obtained. Traditional TOFD yields a single length parameter, while the equivalent flaw time-of-flight diffraction crack sizing method (EFTOFD) described here uses data from multiple look-angles to fit an equivalent degenerate ellipsoid to the crack. The size and orientation of the equivalent flaw can be used to estimate the actual crack size.

Keywords: Ultrasonics, Phased Arrays, Flaw Sizing, Time-of-Flight
PACS: 43.35

INTRODUCTION

Time-of-flight diffraction sizing (TOFD) was developed in the 1970s and is widely used to estimate crack lengths in welds. TOFD uses the time difference Δt between scattered diffraction signals from the crack tips to estimate the length of the crack. Traditionally, the TOFD method is done in a pitch-catch arrangement using single element transducers. No detailed flaw geometry or orientation information is obtained through TOFD sizing, only a single length parameter [1].

A separate time-of-flight-based crack sizing method developed in the 1980s and 1990s used a multi-viewing transducer system, which was composed of multiple conventional transducers arranged conically, to inspect flaws from multiple incident wave directions, or look-angles [2]. A sizing algorithm used the Δt data from different look-angles to estimate the crack size as a best-fit degenerate ellipsoid [3].

This work uses phased array transducers to extend traditional TOFD by incorporating the equivalent flaw sizing algorithm developed with the multi-viewing transducer system. This allows for a single array transducer in pulse-echo or a pair of array transducers in pitch-catch to estimate the size and orientation of a crack in what we will call the equivalent flaw time-of-flight diffraction sizing method, or EFTOFD. The EFTOFD method can be done in nearly the same amount of time as traditional TOFD by making a few more measurements and processing the data with a computationally inexpensive sizing algorithm.

The 39th Annual Review of Progress in Quantitative Nondestructive Evaluation
AIP Conf. Proc. 1511, 895-901 (2013); doi: 10.1063/1.4789139

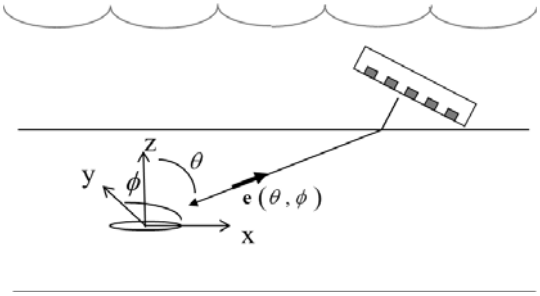

FIGURE 1. Pulse-echo immersion setup for EFTOFD sizing of horizontal crack.

CRACK SIZING ALGORITHM

Figure 1 depicts an immersion, pulse-echo interrogation of a horizontal elliptical crack with a phased array transducer. A coordinate system fixed with respect to the sample with axes x, y, and z can be arbitrarily chosen, and the equivalent flaw size and orientation will be expressed in this coordinate system. To obtain an angle ϕ, the sample can be rotated, or the incident beam can be rotated the same amount in the opposite direction. The beam rotation can be done either by mechanically rotating the transducer or electronically steering the beam. Incident waves from the transducer, with direction given by -**e**, will result in a specularly scattered wave from the crack surface, and two diffracted signals from the crack edges. If the angle θ is such that the specularly reflected wave does not return to the transducer, only the diffracted signals will be seen. Figure 2 shows a simulated A-scan with well separated crack edge diffraction signals. The time difference Δt is defined as the time between the largest peak of the first crack edge signal and the largest peak of the second edge signal. Obtaining a small number of these Δt measurements from different incident vectors $\mathbf{e}(\theta,\phi)$ and solving a linear least squares and eigenvalue problem will allow the determination of an equivalent ellipse.

Schmerr has shown that the Δt data for each **e** is related to the equivalent radius of the ellipse in the direction of **e** [4]. This relationship is given by

$$r_e = c\Delta t/4 \tag{1}$$

and depicted graphically in Fig. 3. Figure 3 shows the incident vector **e** and equivalent radius r_e, along with the semi-major and -minor axes a_1 and a_2 and their directions $\mathbf{u}_1$ and $\mathbf{u}_2$. The direction $\mathbf{u}_3$ corresponds to the crack surface normal. Expressing the equivalent radius in

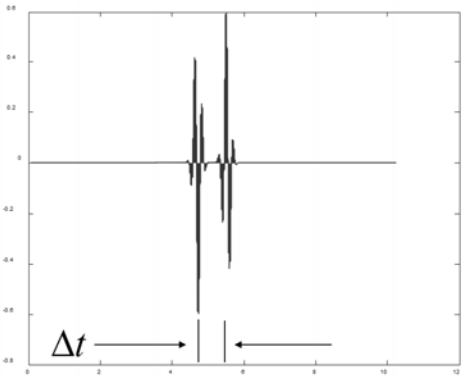

FIGURE 2. Simulated crack edge diffraction signals and the associated Δt.

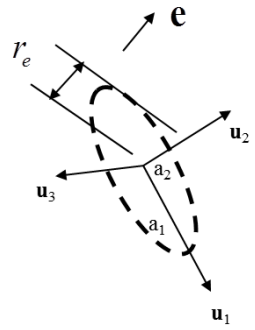

FIGURE 3. Equivalent radius r_e for incident wave direction -**e**.

terms of the incident wave direction -**e** and the ellipsoid parameters $a_1,\ a_2,\ a_3$ and $\mathbf{u}_1,\ \mathbf{u}_2,\ \mathbf{u}_3$ gives [4]

$$r_e^2 = a_1^2(\mathbf{e}\cdot\mathbf{u}_1)^2 + a_2^2(\mathbf{e}\cdot\mathbf{u}_2)^2 + a_3^2(\mathbf{e}\cdot\mathbf{u}_3)^2. \tag{2}$$

Equation (2) can be rewritten as

$$r_e^2(\mathbf{C},\mathbf{e}) = C_{xx}e_x^2 + C_{yy}e_y^2 + C_{zz}e_z^2 + C_{xy}e_xe_y + C_{xz}e_xe_z + C_{yz}e_ye_z \tag{3}$$

where

$$\begin{aligned} C_{xx} &= a_1^2u_{1x}^2 + a_2^2u_{2x}^2 + a_3^2u_{3x}^2 \qquad & C_{xy} &= 2(a_1^2u_{1x}u_{1y} + a_2^2u_{2x}u_{2y} + a_3^2u_{3x}u_{3y}) \\ C_{yy} &= a_1^2u_{1y}^2 + a_2^2u_{2y}^2 + a_3^2u_{3y}^2 \qquad & C_{xz} &= 2(a_1^2u_{1x}u_{1z} + a_2^2u_{2x}u_{2z} + a_3^2u_{3x}u_{3z}) \\ C_{zz} &= a_1^2u_{1z}^2 + a_2^2u_{2z}^2 + a_3^2u_{3z}^2 \qquad & C_{yz} &= 2(a_1^2u_{1y}u_{1z} + a_2^2u_{2y}u_{2z} + a_3^2u_{3y}u_{3z}) \quad . \end{aligned} \tag{4}$$

Using Eqs. (1) and (3) we can define a function, F_m, and error function for M measurements where Δt_m and -$\mathbf{e}_m$ are the m^{th} time difference and incident wave direction, respectively.

$$F_m = \left(\frac{c\Delta t_m}{4}\right)^2 - r_e^2(\mathbf{C},\mathbf{e}_m) \tag{5}$$

$$E(\mathbf{C}) = \sum_{m=1}^{M} F_m^2. \tag{6}$$

Minimizing the error function, i.e.

$$\frac{\partial E}{\partial C_{ij}} = 0 \qquad (i,j = 1,2,3), \tag{7}$$

yields a system of linear equations for the **C** parameters, which can then be used to solve the eigenvalue problem

$$\sum_{j=1}^{3}(C_{ij} - \lambda\delta_{ij})l_j \qquad (i = 1,2,3). \tag{8}$$

It can be shown that the eigenvalues of **C** are just the lengths of the semi-major axes of the equivalent ellipsoid and the eigenvectors are the corresponding directions:

$$\lambda = \begin{pmatrix} a_1^2 \\ a_2^2 \\ a_3^2 \end{pmatrix} \qquad \mathbf{l} = \begin{pmatrix} \mathbf{u}_1 & \mathbf{u}_2 & \mathbf{u}_3 \end{pmatrix}. \tag{9}$$

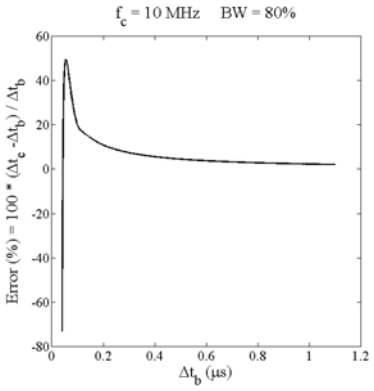

FIGURE 4. Model-based bandwidth error correction curve.

MODEL-BASED BANDWIDTH ERROR CORRECTION

Small Δt measurements are subject to large errors due to the finite bandwidth of the ultrasonic system. These errors can be corrected by using modeling to generate an error correction curve [3], as shown in Fig. 4. The ideal, infinite bandwidth crack edge diffraction signals are modeled using the scattering amplitude given by the Kirchhoff approximation. The exact Δt values, shown as Δt_e in Fig. 4, are taken to be the time differences between these modeled signals. Convolving the Kirchhoff scattering amplitude with a Gaussian distribution, which represents the limited bandwidth of the system, results in a band-limited representation of the diffraction signals. The time differences between peaks of these limited bandwidth signals are taken to be the band-limited Δt values, shown as Δt_b in Fig. 4.

EXPERIMENTAL RESULTS

The experimental setup used is depicted in Fig. 1. Two flaws were used: the first was a #5 flat bottom hole (FBH) with a 1.984 mm diameter in 7075-T651 aluminum, and the second was an elliptical shaped isolated crack-like flaw that was manufactured in a diffusion-bonded titanium sample [5,6]. The elliptical crack was designed to have a semi-major axis of 2.5 mm and a semi-minor axis of 0.6 mm. These flaws are suitable for simulating crack responses because they both exhibit strong edge diffraction signals. The flaws were oriented during

TABLE 1. Data table for 1.984 mm diameter FBH.

θ (deg)	ϕ (deg)	Meas. Δt (μs)	Meas. Δt (μs) with BW Corr.	Exact Δt (μs)
55	0	0.49	0.513	0.5160
50	0	0.45	0.473	0.4826
45	0	0.41	0.433	0.4455
40	0	0.35	0.373	0.4049
40	45	0.36	0.383	0.4049
45	45	0.40	0.423	0.4455
50	45	0.46	0.483	0.4826
55	45	0.50	0.523	0.5160
55	60	0.50	0.523	0.5160
50	60	0.46	0.483	0.4826
45	60	0.41	0.433	0.4455
40	60	0.35	0.373	0.4049

TABLE 2. Data table for 5x1.2 mm (major x minor axes) elliptical crack.

θ (deg)	ϕ (deg)	Meas. Δt (μs)	Meas. Δt (μs) with BW Corr.	Exact Δt (μs)
55	90	0.34	0.362	0.3194
50	90	0.31	0.332	0.2987
45	90	0.26	0.282	0.2757
40	90	0.23	0.252	0.2506
55	60	0.69	0.713	0.7205
50	60	0.63	0.653	0.6738
45	60	0.58	0.603	0.6220
40	60	0.51	0.533	0.5654
40	45	0.66	0.683	0.7593
45	45	0.76	0.783	0.8353
50	45	0.83	0.853	0.9049
55	45	0.93	0.953	0.9676

inspection such that the crack surface normal $\mathbf{u}_3$ was in the z-direction, and the elliptical flaw had the semi-major and -minor axes $\mathbf{u}_1$ and $\mathbf{u}_2$ in the x- and y-directions respectively.

A 32 element, 10 MHz linear array transducer with a 0.36 mm pitch was used to carry out the inspection. The array was used to change the angle θ electronically, while the samples were rotated to change the angle ϕ. Note that the use of a 2-D array would allow both angles to be changed electronically. Twelve look-angles were used for each flaw, and the Δt data can be seen in Table 1 for the FBH and Table 2 for the elliptical crack. The tables show the θ and ϕ values along with the measured Δt values in μs, the bandwidth-corrected measured Δt values, and the exact Δt values obtained through Eq. (2). Cracks with irregular shapes may require additional look-angles over a wider range of angles to estimate the size accurately.

Equation (10) shows the exact results for the FBH, Eq. (11) shows the EFTOFD results with no bandwidth correction, and Eq. (12) shows the EFTOFD results with the bandwidth correction.

$$\begin{pmatrix} a_1 \\ a_2 \\ a_3 \end{pmatrix} = \begin{pmatrix} 0.992 \\ 0.992 \\ 0 \end{pmatrix} \qquad \begin{pmatrix} u_{1x} & u_{2x} & u_{3x} \\ u_{1y} & u_{2y} & u_{3y} \\ u_{1z} & u_{2z} & u_{3z} \end{pmatrix} = \begin{pmatrix} \cdot & \cdot & 0 \\ \cdot & \cdot & 0 \\ 0 & 0 & 1 \end{pmatrix} \tag{10}$$

$$\begin{pmatrix} a_1 \\ a_2 \\ a_3 \end{pmatrix} = \begin{pmatrix} 1.0173 \\ 0.9577 \\ 0.4887i \end{pmatrix} \qquad \begin{pmatrix} u_{1x} & u_{2x} & u_{3x} \\ u_{1y} & u_{2y} & u_{3y} \\ u_{1z} & u_{2z} & u_{3z} \end{pmatrix} = \begin{pmatrix} -0.1500 & -0.9817 & -0.1173 \\ -0.9887 & 0.1481 & 0.0244 \\ 0.0066 & -0.1197 & 0.9928 \end{pmatrix} \tag{11}$$

$$\begin{pmatrix} a_1 \\ a_2 \\ a_3 \end{pmatrix} = \begin{pmatrix} 1.0533 \\ 0.9943 \\ 0.4956i \end{pmatrix} \qquad \begin{pmatrix} u_{1x} & u_{2x} & u_{3x} \\ u_{1y} & u_{2y} & u_{3y} \\ u_{1z} & u_{2z} & u_{3z} \end{pmatrix} = \begin{pmatrix} -0.0741 & -0.9880 & -0.1353 \\ -0.9972 & 0.0729 & 0.0141 \\ 0.0041 & -0.1360 & 0.9907 \end{pmatrix} \tag{12}$$

The dots in Eq. (10) are present because the FBH is circular, and the major and minor axes can be any set of perpendicular directions in the x-y plane.

Equation (13) shows the exact results for the elliptical crack, and Eqs. (14) and (15) show the EFTOFD results without and with the bandwidth correction, respectively.

$$\begin{pmatrix} a_1 \\ a_2 \\ a_3 \end{pmatrix} = \begin{pmatrix} 2.5 \\ 0.6 \\ 0 \end{pmatrix} \qquad \begin{pmatrix} u_{1x} & u_{2x} & u_{3x} \\ u_{1y} & u_{2y} & u_{3y} \\ u_{1z} & u_{2z} & u_{3z} \end{pmatrix} = \begin{pmatrix} 1 & 0 & 0 \\ 0 & 1 & 0 \\ 0 & 0 & 1 \end{pmatrix} \tag{13}$$

$$\begin{pmatrix} a_1 \\ a_2 \\ a_3 \end{pmatrix} = \begin{pmatrix} 2.4594 \\ 0.6255 \\ 0.6928i \end{pmatrix} \quad \begin{pmatrix} u_{1x} & u_{2x} & u_{3x} \\ u_{1y} & u_{2y} & u_{3y} \\ u_{1z} & u_{2z} & u_{3z} \end{pmatrix} = \begin{pmatrix} -0.9821 & -0.0473 & 0.1822 \\ -0.1184 & 0.9076 & -0.4029 \\ 0.1463 & 0.4173 & 0.8969 \end{pmatrix} \quad (14)$$

$$\begin{pmatrix} a_1 \\ a_2 \\ a_3 \end{pmatrix} = \begin{pmatrix} 2.4886 \\ 0.6556 \\ 0.6647i \end{pmatrix} \quad \begin{pmatrix} u_{1x} & u_{2x} & u_{3x} \\ u_{1y} & u_{2y} & u_{3y} \\ u_{1z} & u_{2z} & u_{3z} \end{pmatrix} = \begin{pmatrix} -0.9834 & -0.0581 & 0.1717 \\ -0.1219 & 0.9131 & -0.3890 \\ 0.1342 & 0.4035 & 0.9051 \end{pmatrix} \quad (15)$$

The a_3 values in Eqs. (11), (12), (14), and (15) are imaginary because the a_3^2 values returned by the eigenvalue problem are small, often negative numbers. Taking the square root of a negative value of a_3^2 results in an imaginary a_3. The a_1 and a_2 values for both flaws are estimated to within 10% of their actual values, and the orientation results show good agreement with the expected values. The crack surface normal $\mathbf{u}_3$ for both flaws is estimated as primarily in the z-direction, as expected. Equations (14) and (15) shows that for the elliptical crack the semi-major and -minor axes $\mathbf{u}_1$ and $\mathbf{u}_2$ are predominately along the x- and y-directions, respectively, which was also expected.

The sizing results for these flaws only differ slightly when the bandwidth correction is applied. This is due to most of the Δt values being large enough so that the errors are relatively small. Figure 4 shows that the errors for many of the Δt values encountered are only a few percent. The bandwidth correction becomes more important for smaller flaws, whose smaller Δt values would have much larger errors. However, Table 1 shows that, for the FBH, the Δt values with the bandwidth correction are all closer to the exact values than the Δt values without the correction. Table 2 shows that 10 of the 12 Δt measurements are closer to the exact values with the bandwidth correction than without for the elliptical crack. This trend indicates that the bandwidth correction is removing some systematic error and resulting in more accurate sizing results.

CONCLUSION

The equivalent flaw time-of-flight diffraction (EFTOFD) sizing method has been shown to accurately determine the size and orientation of crack-like flaws using equipment already used for standard TOFD sizing. The inclusion of a few more measurements and a computationally inexpensive processing algorithm allows the EFTOFD method to obtain more quantitative information about the flaw than traditional TOFD sizing. This additional information can be directly used in fracture mechanics studies to determine the significance of the crack from a safety and reliability standpoint.

ACKNOWLEDGMENTS

This work was supported for B.J. Engle and L.W. Schmerr by the NSF Industry/University Cooperative Research Center at Iowa State University, and for A. Sedov by the Natural Sciences and Engineering Research Council of Canada.

REFERENCES

1. J.P. Charlesworth, and J.A.G. Temple, *Engineering applications of time-of-flight diffraction (2nd Ed.)*, Research Studies Press, LTD, (2001).
2. D.O. Thompson, S. Wormley and D. Hsu, "Apparatus and technique for reconstruction of flaws using model-based elastic inverse ultrasonic scattering," *Rev. Sci. Instrum.*, **57**, 3089-3098, (1986).

3. C.P. Chiou and L.W. Schmerr, "New approaches to model-based ultrasonic flaw sizing," *J. Acoust. Soc. Am.*, **92**, 435-444, (1992).
4. L.W. Schmerr, *Fundamentals of Ultrasonic Nondestructive Evaluation – A Modeling Approach*, Plenum Press, New York, N.Y., (1998).
5. B.R. Tittmann and N.E. Paton, "New ultrasonic standards," in *Proceedings of the ARPA/AFML Review of Progress in Quantitative NDE*, AFML-TR-78-55, 1978, pp. 331-335.
6. C.C. Bampton, "Ultrasonic test samples," in *Review of Progress in Quantitative Nondestructive Evaluation 1*, edited by D.O. Thompson and D.E. Chimenti, Plenum Press, New York, NY, 1982, pp. 315-319.